The bond energy of ReO+: Guided ion-beam and theoretical studies of the reaction of Re+ (7S) with O2

P. B. Armentrout

Citation: The Journal of Chemical Physics **139**, 084305 (2013); doi: 10.1063/1.4818642
View online: http://dx.doi.org/10.1063/1.4818642
View Table of Contents: http://scitation.aip.org/content/aip/journal/jcp/139/8?ver=pdfcov
Published by the AIP Publishing

The bond energy of ReO^+: Guided ion-beam and theoretical studies of the reaction of Re^+ (^7S) with O_2

P. B. Armentrout
Chemistry Department, University of Utah, 315 S. 1400 E. Rm 2020, Salt Lake City, Utah 84112, USA

(Received 28 May 2013; accepted 2 August 2013; published online 23 August 2013)

The kinetic-energy dependence of the $Re^+ + O_2$ reaction is examined using guided ion-beam mass spectrometry. The cross section for ReO^+ formation from ground state Re^+ (^7S) is unusual, exhibiting two endothermic features. The kinetic energy dependence for ReO^+ formation is analyzed to determine $D_0(Re^+–O) = 4.82 \pm 0.05$ eV, with the higher energy feature having a threshold 1.35 $\pm$ 0.28 eV higher in energy. This bond energy is consistent with much less precise values determined in the literature. Formation of ReO_2^+ is also observed with a pressure dependent cross section, establishing that it is formed in an exothermic reaction of ReO^+ with O_2. The nature of the bonding for ReO^+ and ReO_2^+ is discussed and analyzed primarily using theoretical calculations at the B3LYP/def2-TZVPPD level of theory. The ground state of ReO^+ is identified as either $^5\Pi$ or $^3\Delta$, with the latter favored once estimates of spin-orbit splitting are included. Bond energies for ground state ReO^+ are calculated at this level as well as BP86 and CCSD(T,full) levels using several different basis sets. BP86 theoretical bond energies are higher than the experimental value, whereas B3LYP and CCSD(T,full) values are lower, although estimated spin-orbit corrections increase the latter close to experiment. Potential energy surfaces for the reaction of Re^+ with O_2 are also calculated at the B3LYP/def2-TZVPPD level of theory and reveal that ground state Re^+ (^7S) inserts into O_2 by forming a $Re^+(O_2)$ ($^5A''$) complex which can then couple with additional surfaces to form ground state ReO_2^+ ($^3B_1$). Several explanations for the unusual dual endothermic features are explored, with no unambiguous explanation being evident. As such, this heavy metal system provides a very interesting experimental phenomenon of both adiabatic and nonadiabatic behavior. © *2013 AIP Publishing LLC*. [http://dx.doi.org/10.1063/1.4818642]

I. INTRODUCTION

Periodic trends in reactivity and thermochemistry are readily studied in the gas phase where the obligations of closed shell structures and solvation are removed. Thus, the gas phase is an ideal venue for determining the energetics of bond-making and bond-breaking processes at a molecular level. One particularly important set of molecules for such studies are transition metal oxides, which can act as models of important oxidation catalysts. The characteristics of such transition metal oxides have been reviewed by Schröder and Schwarz,[1,2] who also summarize what is known about the thermodynamics of these species, information that is critical to understanding, evaluating, and predicting their reactivity. Although the thermochemistry for most transition metal oxides is well established, this is not true for many of the third row transition metal oxides and their cations. In the present work, we seek to remedy this situation for the particular case of ReO^+.

There are few studies of the gas phase oxides of rhenium. For neutral ReO, the 1969 compilation of Brewer and Rosenblatt notes that ReO "has never been observed"[3] and Pedley and Marshall[4] discount the lone experimental measurement at that time from Farber *et al.* (which suggested D(ReO) = 8.2 eV),[5] choosing an estimated bond energy of 6.45 $\pm$ 0.87 eV instead. Battles, Gundersen, and Edwards used high temperature mass spectrometry (HTMS) to investigate the vapor above combinations of Re(s) + ReO_2(s) and ReO_2(s) + ReO_3(s).[6] They found the main gas-phase component to be Re_2O_7 with small amounts of ReO_3. From Re_2O_7(g), an appearance energy for ReO_2^+ of ~20 eV was determined. Similarly, Skinner and Searcy used HTMS to study vapors over Re_2O_7(s) + ReO_3(s), Re_2O_7(s) + ZnO(s), and Re_2O_7(s) + MgO(s), thereby determining the heat of formation of ReO_3(g) and lower limits to those for Re_2O_6(g), ReO_2(g), and ReO(g).[7] Appearance energies for ReO_3^+, ReO_2^+, and ReO^+ from ReO_3(g) were measured as 12.5 $\pm$ 0.4, 14.4 $\pm$ 1.0, and ~18 eV, respectively. Bondybey and co-workers used ion cyclotron resonance mass spectrometry (ICR-MS) to examine several gas-phase rhenium oxide cations, ReO_n^+ where n = 2–6 and 8.[8] In a subsequent study by this group, they performed collision-induced dissociation (CID) studies on all these species, reporting bond energies in most cases, along with density functional calculations of these species in their ground electronic states.[9] At present, this study provides the most accurate thermochemistry for ReO_2^+ and ReO^+, with bond energies for O atom loss of 7.4 $\pm$ 2.2_5 and 5.0 $\pm$ 1.3_5 eV, respectively. Finally, in inductively coupled plasma/selected ion flow tube (ICP/SIFT) experiments by Bohme and co-workers, Re^+ was found to react slowly with O_2 to form ReO_2^+ by three-body association, with subsequent additions of oxygen yielding ReO_n^+ where n = 3–6.[10] The failure to observe reaction (1) at thermal

energies suggests that $D(Re^+–O) < D(O_2) = 5.1$ eV,

$$Re^+ + O_2 \rightarrow ReO^+ + O, \quad (1)$$

as also concluded by Beyer *et al.*[9] Bohme and co-workers also found that Re^+ reacts with NO to form ReO_n^+ where $n = 1 – 4$, which they attributed to sequential termolecular reactions forming N_2O as the neutral product,[11] although this interpretation has been questioned for other metals.[12]

Clearly, the thermochemistry of the rhenium oxide cations is not known very well. The present study is designed to provide more quantitative information about ReO^+ by examining the kinetic energy dependence of reaction (1) using guided ion beam tandem mass spectrometry (GIBMS). This work reveals the energetics, kinetics, and dynamics of the interaction of the rhenium metal cation with O_2. In previous studies in our laboratory, GIBMS has been used to systematically study the kinetic energy dependent reactions of O_2 with atomic cations of the first-row,[13–21] second-row,[15,16,22–27] and third-row transition metals[16,28–33] and main group metals.[34–36] In many cases, analyses of the cross sections for the analogues of reaction (1) have enabled determination of the BDEs of the metal oxide cation, MO^+. The present work extends these studies to include the metal ion Re^+, and as such, is part of an ongoing effort in our laboratory to understand the periodic trends in the BDEs of metal oxides. As will be seen below, the kinetic energy dependent cross section for reaction (1) is unusual, exhibiting two endothermic features, which parallels similar behavior recently observed for the neighboring element, Os^+ reacting with O_2.[33] The reasons behind this behavior are explored in terms of spin-conservation and adiabatic versus nonadiabatic behavior.

II. EXPERIMENTAL AND THEORETICAL

A. General experimental

The guided ion beam tandem mass spectrometer on which these experiments were performed has been described in detail previously.[37,38] Briefly, atomic rhenium ions are generated in a direct current discharge flow tube (DC/FT) source described below, extracted from the source, accelerated, and focused into a magnetic sector momentum analyzer for mass selection of primary ions. The mass-selected ions are decelerated to a desired kinetic energy and focused into an octopole ion beam guide that uses radio-frequency (rf) electric fields to trap the ions in the radial direction and ensure complete collection of reactant and product ions.[39,40] The octopole passes through a static gas cell with an effective length of 8.26 cm that contains the reaction partner (here, O_2) at a low pressure (less than ~0.3 mTorr) so that multiple ion–molecule collisions are improbable. The unreacted parent and product ions are confined radially in the guide until they drift to the end of the octopole where they are extracted, focused, and passed through a quadrupole mass filter for mass analysis of products. Ions are subsequently detected with a secondary electron scintillation ion detector[41] using standard pulse counting techniques. Reaction cross sections are calculated from product ion intensities relative to reactant ion intensities after correcting for background signals.[42] Uncertainties in absolute cross sections are estimated to be ±20%.

The kinetic energy of the ions is varied in the laboratory frame by scanning the dc bias on the octopole rods with respect to the potential of the ion source region. Laboratory (Lab) ion energies are converted to energies in the center-of-mass frame (CM) by using the formula $E_{CM} = E_{lab} \times m/(m + M)$, where m and M are the neutral and ionic reactant masses, respectively. Two effects broaden the cross section data: the kinetic energy distribution of the reactant ion and the thermal motion of the neutral reactant gas (Doppler broadening).[43] The absolute zero and the full width at half maximum (FWHM) of the kinetic energy distribution of the reactant ions are determined using the octopole beam guide as a retarding potential analyzer, as described previously.[42] The distributions of ion energies, which are independent of energy, are nearly Gaussian and have a typical FWHM of 0.4–0.5 eV (Lab) in these studies. Uncertainties in the absolute zero of the energy scale are ±0.1 eV (Lab) and ±0.014 eV (CM).

B. Ion source

Re^+ ions are produced in a dc-discharge/flow tube (DC/FT) ion source,[38] consisting of a cathode held at a high negative voltage (0.7–1.5 kV) over which a flow of approximately 90% He and 10% Ar passes at a total pressure of 0.3–0.5 Torr and ambient temperature. The dc-discharge ionizes Ar and then accelerates these ions into the cathode, which is a rhenium cylinder attached to an iron holder. As the ions are swept down the meter-long flow tube, they undergo ~10^5 thermalizing collisions with He and Ar. As demonstrated earlier,[44,45] trace amounts (<0.1%) of low-lying excited states are observed to survive these flow conditions, but these are easily removed by introducing CH_4 to the flow tube about 15 cm downstream of the discharge zone at a pressure of ~100 mTorr. With the addition of this cooling gas, the DC/FT source produces Re^+ ions in the ground state, as demonstrated in previous studies of Re^+ with H_2, HD, and D_2 and with CH_4 and CD_4.[44,45] When compared to a surface ionization source, the DC/FT source has been found to generate Sc^+,[46] Fe^+,[47] Co^+,[48] Ni^+,[49] Ru^+,[50] Rh^+,[50] and Pd^+[50] ions with an average electronic temperature of 700 ± 400 K, and Y^+, Zr^+, Nb^+, and Mo^+ ions with an average electronic temperature of 300 ± 100 K.[51] In the case of Re^+, even an elevated electronic temperature products a pure beam of $^7S_3$ ($6s^15d^5$) ground state because excited states are too high in energy to be populated. The ^5D first excited state has an energy of 1.827 eV (average over all spin-orbit levels) with the ^5S ($6s^15d^5$) second excited state at 2.135 eV.[52]

C. Data analysis

Cross sections of endothermic reactions are modeled using Eq. (2),[53–56]

$$\sigma(E) = \sigma_0 \sum g_i (E + E_i - E_0)^n / E, \quad (2)$$

where σ_0 is an energy-independent scaling factor, E is the relative kinetic energy of the reactants, n is an adjustable

parameter that characterizes the energy dependence of the process,[53] and E_0 is the 0 K threshold for reaction of electronic, vibrational, and rotational ground state reactants. The model involves an explicit sum of the contributions of individual ro-vibrational states of the room temperature O_2 reactant (ν = 1580 cm^{-1}, B = 1.4456 cm^{-1}),[57] denoted by i, having energies E_i and populations g_i. As noted above, contributions from excited electronic states of Re^+ are zero. Before comparison with the experimental data, Eq. (2) is convoluted with the kinetic energy distributions of the reactant ions and neutrals at 300 K.[42] The σ_0, n, and E_0 parameters are then optimized using a nonlinear least-squares analysis to give the best reproduction of the data. Error limits for E_0 are calculated from the range of threshold values for different data sets over a range of acceptable n values combined with the absolute uncertainty in the kinetic energy scale.

D. Theoretical calculations

Most quantum chemistry calculations reported here were computed using the B3LYP hybrid density functional method and performed with the GAUSSIAN 09 suite of programs.[58] The B3LYP method is based on the hybrid gradient-corrected exchange functional proposed by Becke[59] combined with the gradient-corrected correlation functional of Lee, Yang, and Parr.[60] We also used the BP86 density functional,[61] along with coupled cluster with single, double, and perturbative triple excitations (CCSD(T,full)).[62–65] The BP86 functional is chosen specifically because it was found to perform well for a variety of transition metal complexes[66] and has been found to yield reasonable upper limits on the thermochemistry of organometallic species in previous work, where B3LYP gives reasonable lower limits.[67] The def2-TZVPPD basis set was used for oxygen in most calculations and gives good results for the thermochemistry of O_2 with an O–O bond energy calculated using B3LYP as 5.25 eV, compared to the experimental value of 5.115 eV, Table I.[68] BP86 yields a high value (near 6.1 eV) and even the CCSD(T,full) approach is off somewhat with a bond energy of 4.88 eV. Increasing the size of the basis set to def2-QZVPPD or use of aug-cc-pVxZ basis sets (x = T, Q, 5) leads to excellent agreement for CCSD(T,full) with bond energies of 5.03–5.11 eV, whereas these basis sets affect the results for the two DFT approaches very little, Table I.

For rhenium, several basis sets were used, all using relativistic effective core potentials (ECPs) that are small core (60 electrons) such that the 5s, 5p, 5d, and 6s orbitals are explicitly considered. The def2-TZVPPD and def2-QZVPPD[69] use ECPs developed by Andrea *et al.*[70] We also utilized the energy-consistent pseudopotentials and correlation consistent basis sets developed by Figgen *et al.* (aug-cc-pVxZ-PP where x = T, Q, and 5)[71] along with comparable basis sets on oxygen. For both types of basis sets, the triple and quadruple zeta include f and g type polarization functions on Re, and the quintuple zeta adds h and i functions as well. (The def2 and aug-cc-pVxZ-PP basis sets were obtained from the basis set exchange of the Environmental and Molecular Sciences Laboratory, EMSL.[72,73]) In all cases, the thermochemistry calculated and cited here for ReO^+ and ReO_2^+ is corrected for zero point energy effects, after scaling the frequencies by 0.989.[74] For those systems where the aug-cc-pVxZ basis sets were used, we also performed a complete basis set extrapolation using two-point (Q,5) protocols for both the Hartree-Fock total energy and the CCSD(T) correlation energy, as recommended by Halkier *et al.*[75,76]

TABLE I. Bond energy of O_2 ($^3\Sigma^-$) and $^7S \rightarrow {}^5D$ excitation energy for the atomic rhenium ion (eV) calculated at several levels of theory.

State	Basis set	B3LYP	BP86	CCSD(T,full)	Expt.
$D_0(O_2, {}^3\Sigma_g^-)$	def2-TZVPPD	5.25	6.06	4.88	5.115
	def2-QZVPPD	5.27	6.07	5.04	
	aug-cc-pVTZ	5.24	6.05	5.03	
	aug-cc-pVQZ	5.28	6.08	5.07	
	aug-cc-pV5Z	5.28	6.08	5.11	
	CBS[a]			5.15	
$^7S \rightarrow {}^5D(5d^6)$	def2-TZVPP	2.125	2.319	2.476	1.827[b]
	def2-QZVPP	2.128	2.320	2.454	
	aug-cc-pVTZ	2.145	2.335	2.468	
	aug-cc-pVQZ	2.145	2.335	2.468	
	aug-cc-pV5Z	2.158	2.344	2.408	
	CBS[a]			2.299	
$^7S \rightarrow {}^5D(6s^25d^4)$	def2-TZVPP	2.595	2.793	2.764	1.827[b]
	def2-QZVPP	2.582	2.779	2.746	
	aug-cc-pVTZ	2.576	2.781	2.740	
	aug-cc-pVQZ	2.576	2.781	2.740	
	aug-cc-pV5Z	2.571	2.777	2.755	
	CBS[a]			2.784	

[a]Complete basis set limit.
[b]Statistically weighted mean of spin-orbit levels.

One means of testing the validity of the theoretical results is to compare calculated excitation energies of the various states of Re^+ to experimentally measured values, Table I. Experimentally, the ^5D first excited state has an energy of 1.827 eV (average over all spin-orbit levels) above the $^7S(6s^15d^5)$ ground state with the $^5S(6s^15d^5)$ second excited state at 2.135 eV.[52] (Although Moore identifies the ^5D state as having a $6s^25d^4$ configuration, more recent evaluations indicate mixed character of these five J levels (0–4) including $6s^25d^4$, $6s^15d^5$, and $5d^6$.[77]) The present calculations properly identified the ground state as the ^7S in all cases and find that the $^5D(5d^6)$ state lies ~2.14 (B3LYP), ~2.33 (BP86), and ~2.44 (CCSD(T,full)) eV above the ^7S ground state, whereas excitation to the $^5D(6s^25d^4)$ state requires ~2.58, ~2.78, and ~2.75 eV, respectively (where it was ensured that these states had no spin-contamination), Table I. Lower lying quintet states could also be calculated but these were invariably spin contaminated, s(s + 1) = 6.98 instead of 6. The present results are comparable to previous theoretical results, e.g., Ohanessian *et al.* calculate that the $^5D(5d^6)$ and $^5D(6s^25d^4)$ states lie 2.64 and 2.94 eV above the ^7S ground state;[78] Dai and Balasubramanian calculated an excited $^5G(6s^15d^5)$ state lying at 2.687 eV;[79] and Holthausen *et al.*[80] find a ground state of $^5D(5d^6)$ using the B3LYP and BHLYP functionals, with the ^7S state lying 0.26 and 0.10 eV higher in energy, whereas their QCISD and QCISD(T) calculations provided the correct ordering with quintet excitation energies of 1.11 and 1.09 eV, respectively. Excitation

energies for triplet and singlet states of Re^+ have not been experimentally identified largely because of the extensive spin–orbit coupling for this heavy metal.

III. RESULTS

A. Reaction of Re^+ with O_2

Figure 1 shows cross sections for the reaction of Re^+ with O_2 at a pressure of 0.29 mTorr yielding ReO^+ and $ReO_2{}^+$ as a function of kinetic energy. The ReO^+ cross section exhibits two features. The first feature has an apparent threshold near 0 eV, reaches a maximum near 1 eV and then plateaus. The second feature has an apparent threshold near 1.5 eV, reaches a maximum near 5 eV, and then starts to decline because the ReO^+ product ion can dissociate further in reaction (3),

$$Re^+ + O_2 \rightarrow ReO^+ + O \rightarrow Re^+ + O + O, \qquad (3)$$

which has a thermodynamic threshold of 5.115 eV = $D_0(O_2)$. Notably the endothermicity of reaction (1) observed here agrees with the conclusions of Beyer *et al.*[9] and the failure to observe reaction (1) at room temperature by Bohme and co-workers.[10] Our cross sections for reaction (1) at near thermal energy (0.05 eV) can be converted to a rate coefficient at 300 K of $(5 \pm 2) \times 10^{-13}$ cm^3 molecule^{-1} s^{-1}, three orders of magnitude smaller than the collision limit and small enough to agree with the failure to observe this process in the previous study.

Figure 1 also shows the cross section for the formation of $ReO_2{}^+$. The magnitude of this cross section was found to depend linearly on O_2 pressure, such that it disappears when extrapolated to zero pressure. Thus, this product is formed in the sequential reaction (4),

$$ReO^+ + O_2 \rightarrow ReO_2{}^+ + O, \qquad (4)$$

or by a termolecular association process. We exclude the latter process because Koyanagi *et al.* find the termolecular process

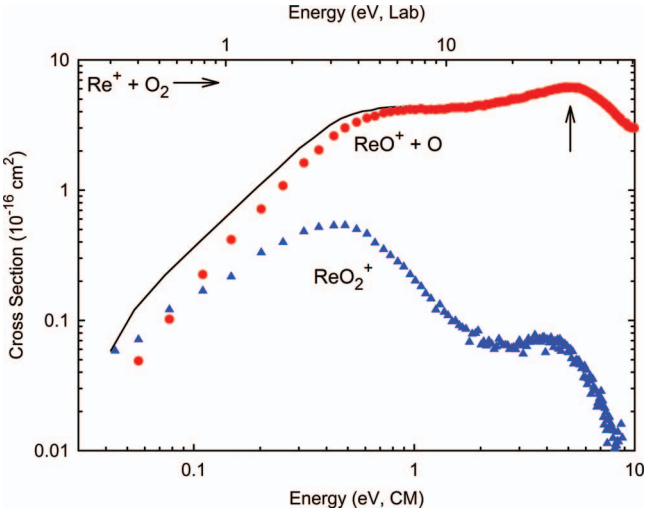

FIG. 1. Cross sections for the reaction of Re^+ (^7S) with O_2 at a pressure of 0.29 mTorr as a function of kinetic energy in the center-of-mass frame (lower axis) and laboratory frame (upper axis). Formation of ReO^+ (circles), $ReO_2{}^+$ (triangles), and their total (line) are indicated. The arrow shows the O_2 bond energy at 5.115 eV.

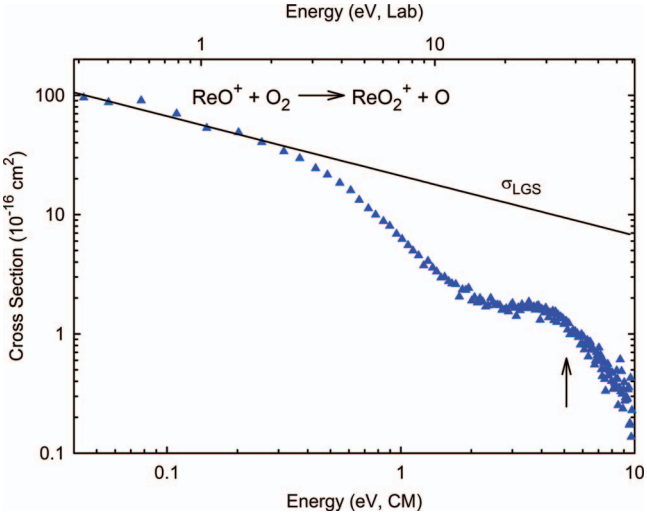

FIG. 2. Estimated cross section for reaction (4) determined as described in the text as a function of kinetic energy in the center-of-mass (lower axis) and laboratory (upper axis) frames. The arrow indicates the O_2 bond energy at 5.115 eV. The line shows the Langevin-Gioumousis-Stevenson collision cross section, Eq. (5).

in He at 0.35 Torr has an apparent bimolecular rate constant of only 1.1×10^{-12} cm^3 s^{-1},[10] such that the termolecular process with an O_2 pressure that is three orders of magnitude smaller would not be observed. More insight into $ReO_2{}^+$ production can therefore be obtained by interpreting the raw data as if the ReO^+ species is the reactant and the intensities are again converted to an absolute cross section. Figure 2 shows the data taken at $P(O_2) = 0.29$ mTorr interpreted in this fashion. Data taken at $P(O_2) = 0.19$, 0.15, and 0.10 mTorr are quantitatively similar in magnitude and energy dependence. It should be realized that this interpretation is not precisely correct in that the kinetic energy of the ReO^+ product is no longer accurately reflected by the energy axis shown (that of the $Re^+ + O_2$ reactants). Nevertheless, the $ReO_2{}^+$ cross section obtained falls off uniformly with energy below 2 eV, with an energy dependence and magnitude below 0.3 eV that matches that expected for ion-neutral collisions according to the Langevin-Gioumousis-Stevenson (LGS) model,[81] Eq. (5),

$$\sigma_{LGS} = \pi e(\alpha/2\pi\varepsilon_0 E)^{1/2}, \qquad (5)$$

where e is the charge on the electron, α is the polarizability volume of the neutral reactant molecule (1.57 Å^3 for O_2),[82] and ε_0 is the permittivity of vacuum. Thus, reaction (4) appears to occur at the collision limit with no barrier.

The cross section for reaction (4) shown in Figure 2 also exhibits a high energy feature starting about 2 eV. Although it is possible that this corresponds to formation of an excited state of $ReO_2{}^+$, it is also plausible that this simply follows from the second feature in the primary ReO^+ product cross section. This latter possibility recognizes the fact that the ReO^+ products formed at threshold in this second feature have little kinetic energy and hence should react efficiently in an exothermic process. This is again a reflection that the energy scale shown may not be accurate.

B. Analysis of the ReO^+ product cross section

The first endothermic feature in the ReO^+ product cross section presumably corresponds to the formation of ground state ReO^+ in reaction (1). This process has an apparent threshold near 0 eV and then plateaus starting around 1 eV before the rise of the second endothermic feature near 1.5 eV. Because the only neutral product that can accompany ReO^+ is atomic O, the second feature is plausibly assigned to the formation of electronically excited products. The energy difference between the two features is smaller than the lowest excitation of the O neutral product, which requires 1.97 eV to form the ^{1}D state.[68] Therefore, we tentatively assign the second cross section feature to the formation of electronically excited ReO^+, an assumption explored further below.

In the low energy region, the total cross section of multiple data sets for the endothermic reaction (1) were analyzed in detail using Eq. (2) as described above, with optimum values of the fitting parameters listed in Table II. A representative model is shown in Figure 3. Because the rotational, vibrational, translational, and electronic energy distributions of the reactants are explicitly included in the modeling, the E_0 thresholds determined using Eq. (2) correspond to 0 K. From the thresholds measured, the ReO^+ BDE at 0 K can be calculated using Eq. (6),

$$D_0(Re^+{-}O) = D_0(O{-}O) - E_0. \quad (6)$$

This equation assumes that there are no activation barriers in excess of the endothermicity of reaction (1), an assumption that is often true for ion-molecule reactions because of the long-range attractive forces.[42,55] This assumption is also confirmed by the theoretical calculations of the potential energy surfaces for this reaction (see below). Thus, from the threshold of 0.29 ± 0.05 eV, Eq. (6) indicates that $D_0(ReO^+) = 4.82 \pm 0.05$ eV. Our bond energy is in good agreement with the much less precise value of $5.0 \pm 1.3_5$ eV determined using CID by Beyer *et al.*[9] When combined with the estimated value for D(ReO) of 6.45 ± 0.87 eV[4] and the ionization energy of Re, IE(Re) = 7.83352 eV,[83] the estimated value for IE(ReO) is 9.46 ± 0.87 eV. This value is comparable to the IEs of other nearby third-row transition metal oxides, 9.1–10.1 eV.[1]

If the models of the low energy feature are extended to higher energies and subtracted from the data, the remaining high energy feature can then be analyzed independently. The high energy feature can be accurately reproduced using Eq. (2) with E_0 = 1.64 ± 0.28 eV, Table II. The difference in the threshold energies is 1.35 ± 0.28 eV. Modeling of the data above 5 eV includes consideration of the decline in the cross section associated with reaction (3). A statistical model for this process includes two parameters: the energy onset for reaction (3), E_D, and a parameter p that controls the shape of the cross section in this region.[34] Here, the data are accurately reproduced when E_D is held to $D_0(O_2) = 5.115$ eV, and $p = 1$. Figure 3 shows that the low-energy feature, the high-energy feature, and the decline in the cross section at high energies are reproduced nicely by these models. Similar reproductions are found for all data sets.

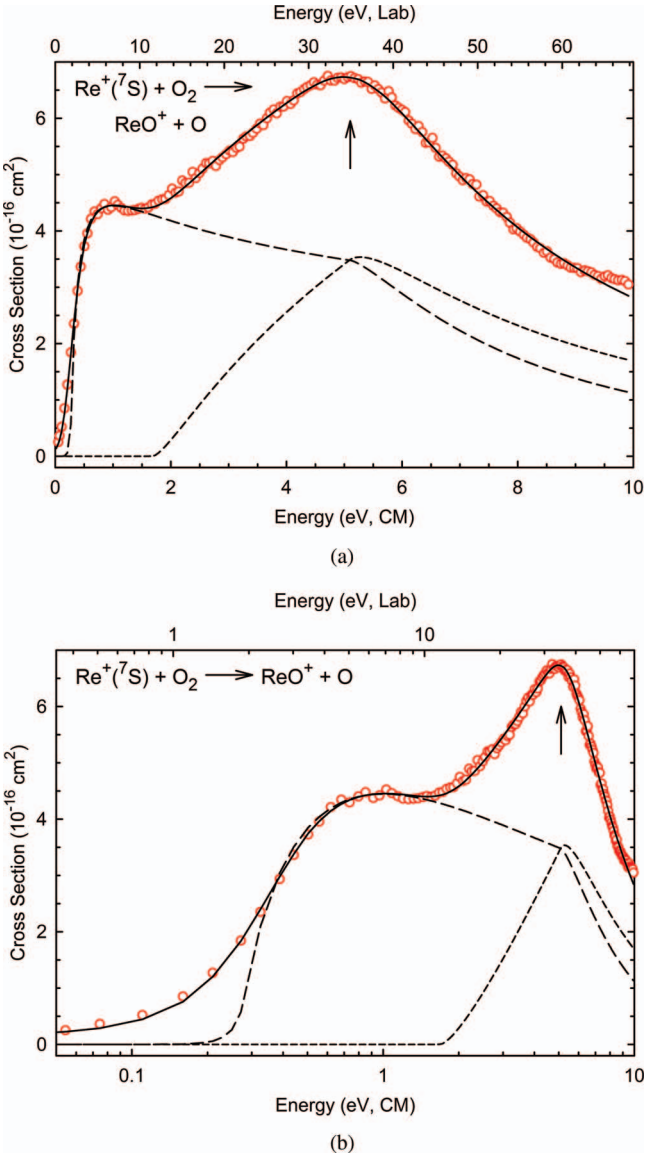

FIG. 3. Zero-pressure extrapolated cross sections for reaction (1) as a function of kinetic energy in the center-of-mass frame (lower axis) and laboratory frame (upper axis) on both linear (part a) and log (part b) scales. The best fits to the data using Eq. (2) with parameters of Table II are shown as dashed lines. The solid lines show the sum of these models convoluted over the kinetic and internal energy distributions of the reactant neutral and ion. The arrows show the O_2 bond energy at 5.115 eV.

TABLE II. Parameters of Eq. (2) used to model reaction (1).[a]

σ_0	n	E_0 (eV)
5.5 ± 0.6	0.8 ± 0.2	0.29 ± 0.05
2.4 ± 0.9	1.5 ± 0.3	1.64 ± 0.28

[a]Uncertainties are two standard deviations.

C. Theoretical results for ReO^+

B3LYP/def2-TZVPPD calculations performed here indicate that the ground state of ReO^+ is $^5\Pi$ with a bond length of 1.679 Å and a valence electron configuration of $1\sigma^2 1\pi^4 1\delta^2 2\sigma^1 2\pi^1$. In this designation of the molecular orbitals (mos), the Re (5*s*, 5*p*), and O (1*s*, 2*s*) core electrons are

TABLE III. Bond lengths, energies, and vibrational frequencies calculated at various levels of theory for ReO^+ ($^5\Pi$), ReO^+ ($^3\Delta$), and ReO^+ ($^1\Sigma^+$).

State	Level	Basis set	r(Re–O) (Å)	E (E_h)	ω_e (cm^{-1})	D_0/E_{rel} (eV)[a]	D_0/E_{rel} (eV)[a] incl. spin-orbit
$^5\Pi$	B3LYP	def2-TZVPPD	1.679	−153.174976	1015	4.42	*0.125*
		def2-QZVPPD	1.678	−153.180051	1014	4.43	*0.129*
		aug-cc-pV5Z	1.671	−153.482727	1022	4.52	*0.141*
	BP86	def2-TZVPPD	1.687	−153.279784	1003	5.23	*0.100*
		def2-QZVPPD	1.686	−153.285250	1001	5.25	*0.101*
		aug-cc-pV5Z	1.679	−153.583863	1008	5.32	*0.112*
	CCSD(T)	def2-TZVPPD	1.687	−152.773144		3.97	*0.003*
		def2-QZVPPD	1.682	−152.857127		4.10	*0.035*
		aug-cc-pV5Z	1.671	−153.252703		4.27	*0.111*
		CBS[b]		−153.339197		4.27	*0.164*
$^3\Delta$	B3LYP	def2-TZVPPD	1.613	−153.174098	1157	*0.033*	4.70
		def2-QZVPPD	1.612	−153.179297	1155	*0.029*	4.72
		aug-cc-pV5Z	1.605	−153.482428	1164	*0.017*	4.82
	BP86	def2-TZVPPD	1.622	−153.277949	1126	*0.058*	5.49
		def2-QZVPPD	1.622	−153.283439	1124	*0.057*	5.51
		aug-cc-pV5Z	1.615	−153.582445	1132	*0.046*	5.59
	CCSD(T)	def2-TZVPPD	1.611	−152.767753		*0.155*	4.13
		def2-QZVPPD	1.607	−152.852940		*0.123*	4.29
		aug-cc-pV5Z	1.600	−153.251314		*0.047*	4.54
		CBS[b]		−153.339753		*−0.006*	*4.59*
$^1\Sigma^+$	B3LYP	def2-TZVPPD	1.607	−153.133104	1175	*1.149*	*1.432*
		def2-QZVPPD	1.606	−153.138432	1173	*1.142*	*1.429*
		aug-cc-pV5Z	1.600	−153.440360	1179	*1.163*	*1.462*
	BP86	def2-TZVPPD	1.617	−153.231763	1139	*1.315*	*1.573*
		def2-QZVPPD	1.616	−153.237356	1137	*1.312*	*1.571*
		aug-cc-pV5Z	1.609	−153.535252	1143	*1.331*	*1.601*
	CCSD(T)	def2-TZVPPD	1.625	−152.740066		*0.910*	*1.071*
		def2-QZVPPD	1.620	−152.825302		*0.876*	*1.069*
		aug-cc-pV5Z	1.610	−153.223430		*0.806*	*1.075*
		CBS[b]		−153.312854		*0.727*	*1.049*

[a]Bond energy to $Re^+(^7S)+O(^3P)$ (roman) or relative energy compared to ground state (italics). Values include corrections for zero point energies (ZPE). CCSD(T,full) values use B3LYP frequencies.
[b]Complete basis set limit.

not included, the 1σ and 1π are the Re—O bonding mos, with 2π and 3σ being the antibonding counterparts. The 1δ is pure Re($5d$) nonbonding and the 2σ is mostly Re($6s$) nonbonding. Given these identifications, the $^5\Pi$ state has six electrons in bonding mos and one in an antibonding mo for a bond order of 2.5.

In addition to the $^5\Pi$ state, there is also a low-lying $^3\Delta$ state that involves moving an electron from the 2π antibonding orbital to the 1δ nonbonding orbital ($1\sigma^2 1\pi^4 1\delta^3 2\sigma^1$), such that it has a bond order of 3 and a shorter bond, 1.613 Å. This triplet state was identified as the ground state in theoretical work by Beyer *et al.*, although it is not apparent whether other spin states were explored.[9] They obtained a bond length of 1.62 Å at the B3LYP/LanL2DZ/D95(d) level of theory. Yao *et al.*[84] examined the $5d$ metal oxides and their singly charged states using nine different density functionals, the Stuttgart/Dresden effective core potential and basis sets (SDD) on the metals,[70] and the 6-311+G(d) basis set on oxygen. They assigned the ground state of ReO^+ as $^3\Sigma^-$ ($1\sigma^2 1\pi^4 1\delta^2 2\sigma^2$) with unidentified singlet states lying 0.22 (0.68) eV and unidentified quintet states lying 1.08 (0.37) eV higher in energy at the B3LYP (BLYP) levels. Recently, Brites *et al.*[85] performed very high level calculations, multireference configuration interaction (MRCI) using the aug-cc-pV5Z-PP basis set and fully relativistic pseudo potential on Re from Figgen *et al.*[71] They identified the $^3\Delta$ as the ground state with $^3\Sigma^-$ and $^1\Sigma^+$ states lying 0.52 and 0.94 eV higher in energy, but do not appear to have considered a $^5\Pi$ state. In our work, the excitation energy of the $^3\Delta$ state is only 0.03 eV at the B3LYP/def2-TZVPP level, such that there is obviously some question as to the true identity of the ground state. To test this, we calculated the $^5\Pi$–$^3\Delta$ excitation energy at several different levels of theory using several different basis sets (including def2-QZVPPD, the aug-cc-pVxZ-PP basis sets where x = T, Q, and 5, and their complete basis set (CBS) extrapolation) with the results compiled in Table III (results for x = T and Q are not listed as these are very similar to those for x = 5). For B3LYP, BP86, and CCSD(T,full) approaches, the $^5\Pi$ remained the ground state for all basis set sizes with excitation energies to the $^3\Delta$ of 0.01–0.16 eV, although at the CBS limit the $^3\Delta$ lies 0.006 eV below the $^5\Pi$.

Complicating the ground state assignment is the spin-orbit splitting of these two states. To explore this issue further, we assume that $E^{so} = A\ \Lambda\ M_S$ with A being the spin-orbit splitting constant, Λ is the orbital angular momentum quantum number, and M_S is the spin quantum number associated

with a particular $\Omega = \Lambda + M_S$ level.[86] E^{so} can also be assigned as equal to $\Sigma\, a_i\, \ell_i \bullet s_i$ where $\ell_i \bullet s_i$ is the dot product of the orbital angular momentum and the spin of electron i and a_i is the spin-orbit parameter for electron i, which we take as approximately equal to ζ_{5d}(Re), the atomic spin-orbit constant for the 5*d* electrons of atomic Re.[86] For the $^5\Pi$ ($\delta^2\sigma^1\pi^1$) state, these expressions lead to E^{so} ($\Omega = 3$) = 2 A($^5\Pi$) = ζ_{5d}(Re)/2, such that A($^5\Pi$) is approximately ζ_{5d}(Re)/4 ~ 2545 cm^{-1}/4 = 636 cm^{-1}. Ignoring any interactions with other states, this places the $^5\Pi_{-1}$ level at 2 × A = 1272.5 cm^{-1} (0.158 eV) below the unperturbed $^5\Pi$ state. For the $^3\Delta$ state, the spin-orbit splitting constant, A($^3\Delta$) should equal ζ_{5d}(Re)/2 = 1272.5 cm^{-1} such that the $^3\Delta_3$ level should lie 2 × A($^3\Delta$) = 2545 cm^{-1} (0.316 eV) below the unperturbed state, the $^3\Delta_2$ level should lie at the unperturbed state energy, and $^3\Delta_1$ should be 2545 cm^{-1} above the unperturbed state (5090 cm^{-1} above $^3\Delta_3$). This approach is nicely validated by spectroscopy on the isoelectronic ReN molecule, where the splitting between the three $^3\Delta$ levels has been measured as 1810 ± 140 and 3080 ± 140 cm^{-1}, for a splitting of 4990 ± 140 cm^{-1} between the $^3\Delta_3$ and $^3\Delta_1$ levels.[87] (Here the energy of the $^3\Delta_2$ is pushed down by interaction with the $^1\Delta_2$ state arising from the same configuration.) In addition, spin-orbit calculations for ReO^+($^3\Delta$) performed at the CASSCF/cc-pV5Z-PP level by Brites *et al.*[85] find A($^3\Delta$) = 1323.4 cm^{-1}, in good agreement with the 1272.5 cm^{-1} estimate here. Thus, including these estimated spin-orbit corrections, the $^5\Pi_{-1} \rightarrow {}^3\Delta_3$ excitation energy should be lowered by 0.158 eV. These estimated spin-orbit corrections mean that the $^3\Delta$ becomes the likely ground state for all calculations and basis sets used, Table III, with the excitation to the $^5\Pi_{-1}$ state ranging from 0.003 to 0.164 eV.

The 0 K bond energy of the $^5\Pi$ state calculated at the B3LYP/def2-TZVPPD level of theory is 4.42 eV, somewhat below the 4.82 ± 0.05 eV experimental value determined above. Use of different basis sets and theoretical approaches (BP86 and CCSD(T,full)) were also explored, with results compiled in Table III. The aug-cc-pVxZ basis sets increase the BDE by about 0.1 eV. The BP86 approach yields BDEs greater than the B3LYP results by ~0.8 eV, whereas the CCSD(T,full) calculations have lower BDEs by 0.25–0.45 eV, with smaller differences for larger basis sets. One possible explanation for discrepancies between experiment and theory is spin-orbit interactions, which are not explicitly included in the present calculations but were estimated above. Experimental and theoretical bond energies are calculated with respect to the Re^+ (^{7}S) state, which has no spin-orbit splitting. As discussed above, the $^3\Delta$ and $^5\Pi$ states of ReO^+ should have first-order spin-orbit splitting that decrease the energies of the Ω = 3 and −1 levels of these states, such that corrected theoretical BDEs for these states should be increased by 0.32 and 0.16 eV, respectively, as indicated in Table III. Now the BDEs for the $^3\Delta_3$ ground state level increase to 4.7–4.8 eV at the B3LYP level, remain 0.8 eV higher for BP86 calculations, and range from 4.1 to 4.6 eV at the CCSD(T,full) level. With this correction, all levels of theory now suggest that the bond energy measured experimentally is that of the $^3\Delta$ state, with BDEs calculated at the B3LYP level being in excellent agreement with experiment, whereas the CCSD(T,full) values are somewhat low and the BP86 values are high, Table III.

Additional singlet, triplet, quintet, and septet excited states of ReO^+ were also located at the B3LYP and CCSD(T,full) levels using the def2-TZVPPD basis set with results listed in Table IV. B3LYP and CCSD(T,full) results are generally similar both in bond lengths and excitation energies. Other states of ReO^+ located have excitation energies of 0.43–3.51 eV above the $^5\Pi$. These excitation energies are in reasonable agreement with the few states previously calculated by Yao *et al.*[84] and Brites *et al.*[85] It can be seen that states identified as having bond orders of 3 have bond lengths of ~1.61 Å. For states having bond orders of 2.5, the bond lengths increase to ~1.67 Å, whereas the states with bond orders of 2 increase to ~1.73 Å. Two states with bond orders of 1.5 have longer bonds, 1.87 and 1.93 Å. Examination of the vibrational frequencies find that they also track

TABLE IV. Electronic configurations, bond orders, bond lengths, energies, and vibrational frequencies calculated at the B3LYP(CCSD(T,full))/def2-TZVPPD level for ReO^+.[a]

State	Configuration	Bond order	r(Re–O) (Å)	E (E_h)	ω_e (cm^{-1})[b]	E_{rel} (eV)[c]
$^5\Pi$	$1\sigma^2 1\pi^4 1\delta^2 2\sigma^1 2\pi^1$	2.5	1.679/*1.687*	−153.174976	1004	0.00/*0.00*
$^3\Delta$	$1\sigma^2 1\pi^4 1\delta^3 2\sigma^1$	3	1.613/*1.611*	−153.174098	1144	0.03/*0.16*
$^3\Sigma^-$	$1\sigma^2 1\pi^4 1\delta^2 2\sigma^2$	3	1.622/*1.619*	−153.159477	1116	0.43/*0.49*
$^3\Phi/\Pi$	$1\sigma^2 1\pi^4 1\delta^3 2\pi^1$	2.5	1.671/*1.686*	−153.148081	1044	0.73/*0.73*
$^1\Sigma^+$	$1\sigma^2 1\pi^4 1\delta^4$	3	1.607/*1.625*	−153.133104	1162	1.15/*0.91*
$^1\Gamma$	$1\sigma^2 1\pi^4 1\delta^2 2\sigma^2$	3	1.618/*1.631*	−153.123106	1138	1.42/*1.24*
$^1\Phi/\Pi$	$1\sigma^2 1\pi^4 1\delta^3 2\pi^1$	2.5	1.666/*1.666*	−153.119138	1045	1.52/*1.72*
$^5\Sigma^+$	$1\sigma^2 1\pi^4 1\delta^2 2\pi^2$	2	1.728/*1.725*	−153.115318	939	1.62/*1.86*
^{3}H	$1\sigma^2 1\pi^4 1\delta^2 2\sigma^1 2\pi^1$	2.5	1.670/[d]	−153.110840	1048	1.75/[d]
$^7\Pi$	$1\sigma^2 1\pi^3 1\delta^2 2\sigma^1 2\pi^2$	1.5	1.934/*1.935*	−153.093766	681	2.19/*2.19*
$^5\Delta$	$1\sigma^2 1\pi^4 1\delta^1 2\sigma^1 2\pi^2$	2	1.740/*1.739*	−153.086048	918	2.41/*2.65*
$^7\Sigma^+$	$1\sigma^1 1\pi^4 1\delta^2 2\sigma^1 2\pi^2$	1.5	1.869/*1.864*	−153.046109	725	3.49/*3.51*

[a]B3LYP and CCSD(T,full).
[b]Vibrational frequency scaled by 0.989.
[c]Relative energies including corrections for zero point energies (ZPE) scaled by 0.989. CCSD(T,full) values use B3LYP frequencies.
[d]Collapses to the $^3\Phi/\Pi$ state at the CCSD(T,full) level.

reasonably well with the bond order, ~1140 cm^{-1} for 3, ~1030 cm^{-1} for 2.5, ~930 cm^{-1} for 2, and ~700 cm^{-1} for 1.5. Finally, although the present calculations should provide useful guidelines for the presence of excited states, they are limited to single configurations and therefore do not address the true multiconfiguration character of these states.

D. Analysis of the ReO_2^+ product cross section

As discussed above, the ReO_2^+ product is formed in the secondary reaction (4). This process appears to be barrierless, as shown in Figure 2. Thus, these results indicate that $D_0(ORe^+–O) > D_0(O–O) = 5.115$ eV. This agrees with the $7.4 \pm 2.2_5$ eV value obtained from CID experiments by Beyer *et al.*[9]

E. Theoretical results for ReO_2^+

The bonding in metal dioxides has been described previously by Kretzschmar *et al.* (although they use x as the symmetry axis with the molecule in the xz plane, such that b_1 (out-of-plane) and b_2 (in-plane) designations are switched compared with the nomenclature adopted here).[88] Here, we utilize conventions recommended previously,[89] in which the molecule has C_{2v} symmetry along the z-axis with the molecule lying in the yz plane. Core electrons on Re (5*s*, 5*p*) and O (1*s*, 2*s*) are not included in these mos. The $1a_1$ orbital is bonding and formed from the $5d_y^2$ orbital of Re and the $2p_z$ of each oxygen atom, thus forming in-plane Re–O π bonds. There are two doubly occupied, σ-bonding mos ($1b_2$ and $2a_1$) resulting from interaction of the Re($5d_{yz}$) and Re($5d_{x2-z2}$) orbitals with in-phase and out-of-phase combinations of the O($2p_y$) orbitals on each oxygen atom. The $1a_2$ and $1b_1$ mos are doubly occupied out-of-plane π-like mos, which involve the Re($5d_{xy}$) and Re($5d_{xz}$) orbitals combined with out-of-phase and in-phase combinations of the O($2p_x$) orbitals, respectively. The $2b_2$ mo, which is mostly nonbonding in character, is formed from an out-of-phase combination of O($2p_z$) orbitals. The $3a_1$ orbital, also largely nonbonding, is a 6*s*-$5d_{x2}$ hybrid along with a little O($2p_y$) character. Higher lying mos include $2b_1$, $4a_1$, $2a_2$, $3b_2$, and $5a_1$, which are antibonding versions of the $1b_1$, $2a_1$, $1a_2$, $1b_2$, and $1a_1$ bonding mos, respectively.

In previous theoretical work on ReO_2^+, Beyer *et al.* located a ground state $^3B_1$, with a $^5B_2$ state having a $Re^+(O_2)$ geometry lying 3.55 eV higher in energy.[9] (They identify these states as $^3B_2$ and $^5B_1$, respectively, apparently using the same designations as Kretzschmar *et al.*) For ReO_2^+, our calculations also find a $^3B_1$ ground state with equal Re–O bond lengths of 1.669 Å and a bond angle of 112.0°, geometrical parameters that match those of Beyer *et al.*,[9] Table V. The valence electronic configuration of this state is $1a_1^2 1b_2^2 1a_2^2 2a_1^2 1b_1^2 2b_2^2 3a_1^1 2b_1^1$. From this configuration, the $^3B_1$ state has ten electrons in bonding and 1 electron in an antibonding mo such that each ReO bond has a bond order of 2.25. This is reasonable when one compares the 1.669 Å bond length with those listed for the ReO^+ species having bond orders of 2.5, Table IV. Further, this bond order characterization is commensurate with the bond energy. At the B3LYP/def2-TZVPPD level of theory, the $^3B_1$ state is calculated to lie

TABLE V. Bond lengths (Å), bond angles (°), and energies calculated at the B3LYP/def2-TZVPPD level for ReO_2^+.[a]

State	Configuration	r(Re–O)	∠OReO	r(O–O)	∠ReOO	E (E_h)	ZPE (E_h)	E_{rel} (eV)
$^3B_1$	$1a_1^2 1b_2^2 1a_2^2 2a_1^2 1b_1^2 2b_2^2 3a_1^1 2b_1^1$	1.669	112.0			−228.489618	0.005569	0.00
		1.67	*112.3*				*0.005557*	*0.00*
$^1A_1$	$1a_1^2 1b_2^2 1a_2^2 2a_1^2 1b_1^2 2b_2^2 3a_1^2$	1.659	107.4			−228.486059	0.005654	0.10
$^3A_1$	$1a_1^2 1b_2^2 1a_2^2 2a_1^2 1b_1^2 2b_2^2 3a_1^1 4a_1^1$	1.680	115.6			−228.454431	0.005344	0.95
$^3A_2$	$1a_1^2 1b_2^2 1a_2^2 2a_1^2 1b_1^2 2b_2^2 3a_1^1 2a_2^1$	1.687	97.4			−228.435543	0.005751	1.48
$^1A_1$	$1a_1^2 1b_2^2 1a_2^2 2a_1^2 1b_1^2 2b_2^2 2b_1^2$	1.680	122.7			−228.430936	0.005407	1.59
$^5A''(A_2)$	$1a_1^2 1b_2^2 1a_2^2 2a_1^2 1b_1^2 2b_2^1 3a_1^1 2b_1^1 4a_1^1$	1.660, 1.849	135.2			−228.407763	0.004200	2.19
$^1A_2$[b]	$1a_1^2 1b_2^2 1a_2^2 2a_1^2 1b_1^2 2b_2^1 3a_1^1 2b_1^1 4a_1^1$	1.727	137.6			−228.389553	0.002515	2.64
$^5A_1$	$1a_1^2 1b_2^2 1a_2^2 2a_1^2 1b_1^2 2b_2^1 3a_1^1 2b_1^1 2a_2^1$	1.754	93.1			−228.384939	0.003448	2.79
$^3B_2$	$1a_1^2 1b_2^2 1a_2^2 2a_1^2 1b_1^2 2b_2^1 3a_1^2 4a_1^1$	1.729	110.1			−228.371307	0.002864	3.15
$^5B_1$	$1a_1^2 1b_2^2 1a_2^2 2a_1^2 1b_1^2 2b_2^1 3a_1^1 2a_2^1 4a_1^1$	1.771	84.4			−228.360760	0.005584	3.51
$^1B_2$	$1a_1^2 1b_2^2 1a_2^2 2a_1^2 1b_1^2 2b_2^1 3a_1^2 4a_1^1$	1.719	122.2			−228.354523	0.003185	3.61
$^5B_2$	$1a_1^2 1b_2^2 1a_2^2 2a_1^2 1b_1^2 3a_1^1 2b_1^1 2a_2^1 4a_1^1$	1.870	45.2	1.439	67.4	−228.350264	0.005109	3.78
		1.88		*1.43*			*0.005066*	*3.55*
$^5A''(B_1)$	$1a_1^2 1b_2^2 1a_2^2 2a_1^1 1b_1^2 2b_2^2 3a_1^1 2b_1^1 4a_1^1$	1.897, 2.638	27.0	1.282	110.6	−228.324636	0.004132	4.45
$^3B_1$	$1a_1^2 1b_2^2 1a_2^2 2a_1^2 1b_1^2 3a_1^2 2b_1^1 4a_1^1$	1.916	40.7	1.332	69.7	−228.315369	0.004587	4.72
$^7A''(B_1)$	$1a_1^2 1b_2^2 1a_2^1 2a_1^1 1b_1^2 2b_2^2 3a_1^1 2b_1^1 2a_2^1 4a_1^1$	1.956, 2.396	33.2	1.312	92.2	−228.315023	0.004465	4.72
$^1A'(A_1)$	$1a_1^2 1b_2^2 1a_2^2 2a_1^2 1b_1^2 3a_1^2 4a_1^2$	1.845, 1.850	45.8	1.439	66.9	−228.314751	0.004930	4.74
$^9\Sigma^-$	$1\sigma^2 1\pi^4 2\sigma^1 2\pi^2 1\delta^2 3\sigma^1 3\pi^2$	2.949, 4.152	0.0	1.203	180.0	−228.308621	0.004029	4.88
$^7A_2$	$1a_1^2 1b_2^2 1a_2^1 2a_1^2 1b_1^2 2b_2^1 3a_1^1 2b_1^1 2a_2^1 4a_1^1$	1.890	65.2			−228.299343	0.003714	5.13
$^7A''(B_1)$	$1a_1^2 1b_2^2 1a_2^2 2a_1^2 1b_1^1 2b_2^1 3a_1^1 2b_1^1 2a_2^1 4a_1^1$	1.687, 2.451	143.1			−228.297371	0.002970	5.16
$^7B_1$	$1a_1^2 1b_2^2 1a_2^2 2a_1^2 1b_1^1 2b_2^1 3a_1^1 2b_1^1 2a_2^1 4a_1^1$	1.898	127.5			−228.294647	0.003224	5.24
$^7A_1$	$1a_1^2 1b_2^2 1a_2^1 2a_1^2 1b_1^1 2b_2^2 3a_1^1 2b_1^1 2a_2^1 4a_1^1$	1.924	127.5			−228.286502	0.003573	5.47

[a]Values in italics are from Beyer *et al.*[9]

[b]Has an imaginary asymmetric stretch (604 cm^{-1}) and collapses to the $^1A_1$ state.

5.00 eV below the $Re^+(^7S) + O_2$ reactant asymptote and to have a $D_0(ORe^+–O)$ BDE of 5.83 eV. This theoretical value compares favorably to the experimental limit of >5.12 eV (measured here) and the CID value of 7.4 ± 2.2_5 eV of Beyer *et al.*[9]

Table V lists the geometries and energies of various stable states of rhenium dioxide cations, $OReO^+$, calculated at the B3LYP/def2-TZVPPD level of theory. The first excited state of ReO_2^+ is calculated to be a $^1A_1$ state lying 0.10 eV above the ground state, having Re^+–O bond lengths of 1.659 Å, and a OReO angle of 107.4°. This state is formed by moving an electron from the $2b_1$ to the $3a_1$ orbital, such that the ReO bonds have a bond order of 2.5, consistent with the slightly shorter bond length. Other excited states with C_{2v} symmetry were located with excitation energies of 0.95–5.47 eV above the ground state, bond lengths of 1.68–1.92 Å, and bond angles of 40.7°–127.5°. Two states are found to break C_{2v} symmetry by extending one of the Re–O bonds. The $^5A''$ and $^7A''$ states, which would have $^5A_2$ and $^7B_1$ designations if the bond lengths were equal, have one short Re–O bond similar to those of the ReO^+ diatomic, and one much longer bond, 1.85 and 2.45 Å, respectively.

Two of the C_{2v} states, $^5B_2$ and $^3B_1$, are better characterized as adducts of Re^+ with O_2. These are typified by small OReO bond angles (<45°), short OO bond distances (1.33 and 1.44 Å compared to free O_2 at 1.204 Å), and larger Re–O bond lengths (1.87 and 1.92 Å) than the dioxides. The lowest of these, the $^5B_2$ state, was previously located by Beyer *et al.*, with similar bond lengths and excitation energy,[9] Table V. Three additional adduct states have C_s symmetry with unequal Re–O bond lengths. We also located a state having nonet spin, which corresponds to high spin coupling of the $Re^+(^7S) + O_2(^3\Sigma_g^-)$ reactants. This species is linear with a very long Re–O bond, 2.948 Å, such that the O_2 bond is nearly unperturbed, 1.203 Å. This species presumably has a purely electrostatic bond and is only 0.11 eV below the reactants.

F. Potential energy surfaces for $Re^+ + O_2$ on the way to forming $ReO^+ + O$

Calculated potential energy surfaces for the interaction of Re^+ with O_2 ($^3\Sigma_g^-$) are shown in Figures 4(a) and 4(b). They are separated into surfaces having A′ and A″ symmetry as only curves within these groups will strongly interact under experimental conditions for this triatomic system, which necessarily has a plane of symmetry. In most cases, species have C_{2v} symmetry throughout. In the interaction between Re^+ (^7S,A_1,A′) with O_2 ($^3\Sigma_g^-$,B_1,A″), the first step is formation of an association complex intermediate, $Re^+(O_2)$ ($^5A''$) on the A″ surfaces, which has an energy 0.54 eV below the Re^+ (^7S) + O_2 ($^3\Sigma_g^-$) asymptote. This intermediate has ReO bond lengths of 1.897 Å, an OO bond length of 1.282 Å, and bond angles of ∠OReO = 27.0° and ∠ReOO = 110.6°. As the OReO bond angle gets larger, the potential energy surfaces evolve into the more strongly bound rhenium dioxide cationic species, with the $^1A_1$ and $^3B_1$ states being the lowest in energy on the A′ and A″ surfaces, respectively. Note that singlet and triplet states of ReO_2^+ cannot be formed in spin-allowed processes from the ground state Re^+ (^7S) + O_2 ($^3\Sigma_g^-$) reactants and therefore can only be accessed by a curve crossing with one of the quintet or septet surfaces. Importantly, all of the ReO_2^+ surfaces except those of the high-spin septets have minima that lie below the ReO^+ + O product asymptote, calculated to be 0.83 eV (0.55 eV including estimated

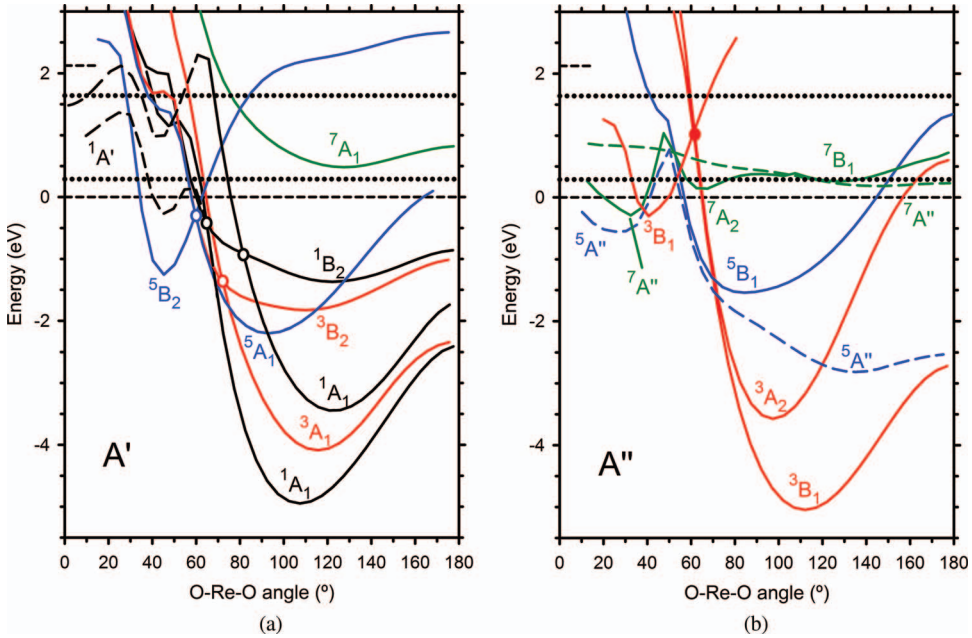

FIG. 4. B3LYP/def2-TZVPPD calculations of the potential energy surfaces for the interaction of Re^+ with O_2 in C_{2v} symmetry as a function of the O–Re^+–O bond angle in degrees. The surfaces are separated into A′ (a) and A″ (b) symmetry with singlet, triplet, quintet, and septet states indicated by black, red, blue, and green lines, respectively. Species having C_{2v} symmetry are shown by full lines and those with C_s symmetry are dashed lines. Horizontal lines indicate the experimental energy zero, corresponding to the Re^+ (^7S) + O_2 ($^3\Sigma_g^-$) reactants at 0.0 eV, and Re^+(^5D) reactant at 2.125 eV, along with dashed lines showing the two experimental energy thresholds determined for formation of ReO^+ + O products, 0.29 and 1.64 eV above the reactants. Circles indicate avoided crossings in C_{2v} (filled) and C_s (open) symmetry.

spin-orbit energies) above the $Re^+ + O_2$ asymptote at this level of theory (0.29 ± 0.05 eV experimentally). Using the CCSD(T,full)/def2-QZVPPD(aug-cc-pV5Z) approaches, the calculated endothermicity is 0.94 (0.84) eV, which shifts to 0.75 (0.57) eV after including estimated spin-orbit energies.

Notably, the A′ surfaces cannot be accessed from ground state reactants within the Born-Oppenheimer approximation. Low-energy pathways leading to the ReO_2^+ intermediates are available on the A″ surfaces, but even here there appears to be a surface crossing point that lies above the energy of the reactants, namely that between the small-angle $^3B_1$ and $^5B_1$ surfaces. This crossing occurs near ∠OReO = 54° at an energy calculated to be 0.42 eV above ground state reactants. It was verified that both surfaces have very similar geometries at this point, with ReO bond lengths of 1.84 Å, such that the surfaces actually do intersect at this point. Importantly, this energy remains below that calculated for ground state products, 0.83 eV, and conceivably could lie lower as a result of spin-orbit coupling associated with the $Re^+(^5D) + O_2(^3\Sigma_g^-)$ reactants that couple to form the $^3B_1$ surface. Given these observations, the energy of this surface crossing seam should not influence the threshold observed for product formation.

Formation of ReO^+ ($^3\Delta$) + O (^{3}P) products should be able to evolve in spin-allowed pathways from several of the singlet, triplet, and quintet ReO_2^+ species and ReO^+ ($^5\Pi$) + O (^{3}P) can be formed from triplet, quintet, and septet intermediates. Indeed, explicit calculations of the surfaces for ORe^+–O bond cleavage from the lowest ReO_2^+ states of singlet, triplet, and quintet spin show no reverse activation barriers, with the latter two states correlating with dissociation to ReO^+ ($^3\Delta$) + O(^{3}P). These dissociation pathways require breaking C_{2v} symmetry such that they are not conveniently shown in Figures 4(a) and 4(b). Thus, the experimentally measured threshold should correspond to the asymptotic limit for formation of ReO^+ + O, thereby yielding accurate thermochemistry for ReO^+.

IV. DISCUSSION

The behavior observed for reaction (1), Figures 1 and 3, is unusual in that two endothermic features are observed. Although it is energetically possible to form excited states in most ion-molecule reactions at elevated kinetic energies, it is unusual for individual product states to give rise to distinct features in GIB experiments, although such behavior has been observed in several previous studies, as discussed below. Clearly, the routes to the two products in question must differ in some fundamental way. Several plausible explanations are discussed here, although it will be seen that none appear to be definitive in the present case.

(1) One potential explanation for the two features is the presence of excited states of Re^+. We discount this possibility because no evidence for such excited states is observed in other systems, reactions with H_2 and CH_4.[44,45] Further, addition of a quenching gas (CH_4) to the source region yielded no change in the cross sections observed.

(2) The high energy feature could correspond to formation of ground state O (^{3}P) at low energies and O (^{1}D) at high energies. However, the excitation energy of 1.35 ± 0.28 eV measured here is well below the 1.97 eV associated with this excitation.[68]

(3) In previous work, two endothermic features were observed in the cross section for formation of VS^+ from reaction of V^+ with CS_2[90] and attributed to reactions (7) and (8).

$$V^+(^5D) + CS_2\left(^1\Sigma_g^+\right) \rightarrow VS^+(^3\Sigma^-) + CS(^1\Sigma^+), \quad (7)$$

$$\rightarrow VS^+(^5\Pi) + CS(^1\Sigma^+). \quad (8)$$

Here formation of the VS^+ ($^3\Sigma^-$) ground state is spin forbidden and formation of VS^+ ($^5\Pi$) is spin-allowed. This distinction can explain why the latter process is easily observed as a distinct feature in the cross section even though it is much more endothermic than the former process. Therefore, the two features observed here for reaction (1) are plausibly assigned to an overall spin-forbidden reaction at low energy and an overall spin-allowed process at high energies, thus forming two different electronic states of the ReO^+ product ion. Belying this explanation is the fact that both reactions (9) and (10) are spin-allowed,

$$Re^+(^7S) + O_2(^3\Sigma_g^-) \rightarrow ReO^+(^3\Delta) + O(^3P), \quad (9)$$

$$\rightarrow ReO^+(^5\Pi) + O(^3P), \quad (10)$$

such that formation of ground state products (no matter what their identity) from ground state reactants is spin-allowed. Indeed, formation of any ReO^+ product state except singlets is spin-allowed, as septet, quintet, and triplet states of ReO^+ along with O(^{3}P) can be formed via quintet intermediates. Furthermore, it seems unlikely that spin is a very good quantum number for this heavy element system.

Nevertheless, we can pursue this idea further by comparing the experimental excitation energy of 1.35 ± 0.28 eV with the theoretical excitation energies in Table IV. In this energy range, there is both a $^1\Sigma^+$ state at 1.15 eV and a $^5\Sigma^+$ state at 1.62 eV, although these values change to 1.43 and 1.91 eV, respectively, when approximate spin-orbit corrections are made (and higher energy fine structure levels of the $^3\Phi/\Pi$ state also move within the experimental energy band). (At the CCSD(T,full)/def2-QZVPPD level(CBS) levels of theory, the $^1\Sigma^+$ state excitation energy is 0.88 (0.73) eV, 1.07 (1.05) eV after spin-orbit corrections, Table III.) As the lowest lying singlet in Table IV, the former state is unique. Notably, reaction (11) is truly spin-forbidden and therefore requires coupling between quintet and triplet surfaces:

$$Re^+(^7S) + O_2(^3\Sigma_g^-) \rightarrow ReO^+(^1\Sigma^+) + O(^3P). \quad (11)$$

Thus, this singlet state is plausibly assigned to the high energy feature observed experimentally; however, it

remains unclear why formation of this state should lead to a unique experimental signature, and especially why a spin-forbidden reaction would be favored at high kinetic energies.

(4) Another reaction for which two endothermic features were observed is $S^+ (^4S) + H_2 \rightarrow SH^+ (^3\Sigma^-) + H (^2S)$.[91] Here, the higher energy feature could be explained as a spin-allowed reaction along a quartet surface exhibiting a barrier, whereas the lower energy feature requires changing to the doublet surface associated with the ground state of the $H_2S^+ (^2B_1)$ intermediate. If the $Re^+ + O_2$ behaved similarly, then reaction at low collision energies could form the ground state $ReO_2^+ (^3B_1)$ intermediate or perhaps the low-lying $ReO_2^+ (^1A_1)$, which are technically spin-forbidden processes from ground state reactants. These intermediates could then dissociate to form either $ReO^+ (^3\Delta)$ or $ReO^+ (^5\Pi) + O(^3P)$. However, these same products could also be formed from quintet states of ReO_2^+ that can be formed from ground state reactants in spin-allowed processes. Furthermore, this scenario does not provide a clear explanation for the origins of the higher energy cross section feature.

(5) An intriguing possibility focuses on the character of the surfaces in the entrance channel, which is effectively shown in Figures 4(a) and 4(b) at small OReO bond angles. For ground state reactants, only $^5A''$, $^7A''$, and $^9A''$ surfaces evolve from ground state reactants with the low-spin $^5A''$ being the most attractive and $^9A''$ being largely repulsive. As shown in Figure 4(b), this $^5A''$ surface crosses surfaces of other spin leading to stable ReO_2^+ intermediates including the $^3B_1$ ground state. Along these surfaces, there is potentially a small barrier to form $ReO_2^+ (^3B_1)$ in excess of the reactant energy where the small angle $^3B_1$ and $^5B_1$ surfaces cross. There should be no barriers for dissociation to $ReO^+ + O$ in excess of the product asymptotic energy. Thus, at low kinetic energies, the reactants pass slowly through the crossing regions, allowing the electrons to adjust to different configurations along the reaction coordinate. Under such conditions, spin inversion can be efficient, and adiabatic behavior is expected. However, all of these surfaces exhibit avoided crossings with surfaces evolving from higher energy reactant states, such that as the nuclear motion speeds up at elevated collision energies, the reactants pass more quickly through the crossing regions, the electrons have less time to adapt, and the Born-Oppenheimer approximation begins to fail. Thus, as the kinetic energy of the reactants increases, it becomes increasingly likely that the reactants will behave diabatically during the collision event and remain on the surface associated with the electron configuration of the ground state reactants. This could lead to a higher barrier to the reaction, observed experimentally as the second cross section feature.

Intriguingly, the surfaces of A′ symmetry (which cannot be accessed adiabatically from ground state reactants) are qualitatively different in the entrance channel. Here, no low-energy pathways are found because they can only evolve from $Re^+(^5D) + O_2(^3\Sigma_g^-)$ or higher energy reactants. Coupling of the A′ and A″ surfaces can occur at elevated kinetic energies by electronic-rotational (Coriolis) coupling, as previously observed for reactions of state-specific rare gas cations (Ar^+, Kr^+, and Xe^+) with H_2, D_2, and HD in the vicinity of 1–2 eV relative kinetic energies.[42,92,93] Coriolis coupling occurs when high rotational velocities of the collision plane of the reactants cause the electrons to "lag" out of the plane. Thus, one possibility is that the low energy behavior observed experimentally corresponds to adiabatic reactions along the A″ surfaces, and the high energy feature observed experimentally is associated with reactions along the A′ surfaces with possible contributions from diabatic pathways on A″.

In evaluating these various possibilities, it is important to note that the related $Os^+ + O_2 \rightarrow OsO^+ + O$ reaction also exhibited two distinct endothermic features,[33] presumably for the same intrinsic reasons. In addition, the $Ir^+ + O_2 \rightarrow IrO^+ + O$ reaction shows similar behavior, although more subtly.[94] There too, specific considerations of the five explanations above were applied with similar unsatisfying results. In all three systems, the observed experimental behavior appears most likely to be associated with adiabatic behavior at low energies followed by some sort of nonadiabatic behavior at higher energies. It seems odd that such behavior is observed for these heavy metal systems where spin is no longer likely to be a very good quantum number, whereas lighter congeners do not exhibit such dual thresholds.[19,22,95] Assuming that spin need not be conserved, the singlet, triplet, quintet, and septet surfaces shown in Figures 4(a) and 4(b) should couple efficiently, such that reaction (1) is controlled by effects in the entrance channel with explanation 5 above providing the most plausible path for the Re^+, Os^+, and Ir^+ systems.

V. CONCLUSION

The kinetic-energy dependence of the $Re^+ + O_2$ reaction is examined using guided ion beam tandem mass spectrometry. The cross section for ReO^+ formation exhibits distinct endothermic features with thresholds measured to be 0.29 ± 0.05 and 1.64 ± 0.28 eV. The former threshold yields a bond energy for ReO^+ of 4.82 ± 0.05 eV, which agrees well with previous imprecise experimental values. Formation of ReO_2^+ was also observed in an exothermic secondary process, leading to thermochemistry in agreement with the literature.

Detailed quantum mechanical calculations are performed for ReO^+ and ReO_2^+ species. The nature of the bonding is analyzed at the B3LYP, BP86, and CCSD(T,full) levels of theory. Basis sets for the metal include def2-QZVPPD, def2-TZVPPD, aug-cc-pVxZ-PP (x = T, Q, 5) and small core relativistic effective core potentials with def2 and aug-cc-pVxZ basis sets used for oxygen. Reasonable agreement between theoretical and experimental bond energies is found for most levels of theory, with B3LYP and CCSD(T,full) being on the low side and BP86 being on the high side. The calculated ground state of ReO^+ is either $^5\Pi$ or $^3\Delta$, although additional consideration of spin-orbit effects suggests that the $^3\Delta$ is the probable ground state. Potential energy surfaces for the

interaction of Re^+ with O_2 are also calculated at the B3LYP/def2-TZVPPD level of theory. These surfaces demonstrate that Re^+ inserts into O_2 to form ground state ReO_2^+ via a curve crossing model and that ground state ReO^+ can be formed with no barriers in excess of endothermicity, consistent with the experimental results.

Several possible reasons for the unusual behavior observed here and for the analogous reactions of Os^+ and Ir^+ are explored, but no completely satisfying explanation evolves. It seems clear that these heavy metal systems exhibit both adiabatic behavior at low collision energy followed by nonadiabatic behavior at higher energies, but the detailed nature of the nonadiabatic behavior is not evident.

ACKNOWLEDGMENTS

This research is funded by the National Science Foundation under Grant No. CHE-1049580. Feng-Xia Li is thanked for acquiring the experimental data. Professor Michael D. Morse is thanked for several very helpful discussions, especially regarding spin-orbit coupling.

[1]D. Schröder and H. Schwarz, Angew. Chem., Int. Ed. Engl. **34**, 1973 (1995).
[2]D. Schröder, H. Schwarz, and S. Shaik, Struct. Bonding **97**, 91 (2000).
[3]L. Brewer and G. M. Rosenblatt, in *Advances in High Temperature Chemistry*, edited by L. Eyring (Academic, New York, 1969), Vol. 2, p. 1.
[4]J. B. Pedley and E. M. Marshall, J. Phys. Chem. Ref. Data **12**, 967 (1983).
[5]M. Farber, S. P. Harris, and R. D. Srivastava, Combust. Flame **22**, 191 (1974).
[6]J. E. Battles, G. E. Gundersen, and R. K. Edwards, J. Phys. Chem. **72**, 3963 (1968).
[7]H. B. Skinner and A. W. Searcy, J. Phys. Chem. **77**, 1578 (1973).
[8]M. Beyer, C. Berg, G. Albert, U. Achatz, S. Joos, G. Niedner-Schatteburg, and V. E. Bondybey, J. Am. Chem. Soc. **119**, 1466 (1997).
[9]M. Beyer, C. Berg, S. Joos, U. Achatz, W. Hieringer, G. Niedner-Schatteburg, and V. E. Bondybey, Int. J. Mass Spectrom. **185–187**, 625 (1999).
[10]G. K. Koyanagi, D. Caraiman, V. Blagojevic, and D. K. Bohme, J. Phys. Chem. A **106**, 4581 (2002).
[11]V. Blagojevic, E. Flaim, M. J. Y. Jarvis, G. K. Koyanagi, and D. K. Bohme, J. Phys. Chem. A **109**, 11224 (2005).
[12]J. J. Melko, S. G. Ard, J. A. Fournier, N. S. Shuman, J. Troe, and A. A. Viggiano, J. Phys. Chem. A **116**, 11500 (2012).
[13]N. Aristov and P. B. Armentrout, J. Phys. Chem. **90**, 5135 (1986).
[14]S. K. Loh, E. R. Fisher, L. Lian, R. H. Schultz, and P. B. Armentrout, J. Phys. Chem. **93**, 3159 (1989).
[15]S. K. Loh, L. Lian, and P. B. Armentrout, J. Chem. Phys. **91**, 6148 (1989).
[16]D. E. Clemmer, N. F. Dalleska, and P. B. Armentrout, Chem. Phys. Lett. **190**, 259 (1992).
[17]D. E. Clemmer, N. F. Dalleska, and P. B. Armentrout, J. Chem. Phys. **95**, 7263 (1991).
[18]D. E. Clemmer, J. L. Elkind, N. Aristov, and P. B. Armentrout, J. Chem. Phys. **95**, 3387 (1991).
[19]E. R. Fisher, J. L. Elkind, D. E. Clemmer, R. Georgiadis, S. K. Loh, N. Aristov, L. S. Sunderlin, and P. B. Armentrout, J. Chem. Phys. **93**, 2676 (1990).
[20]M. R. Sievers and P. B. Armentrout, J. Chem. Phys. **102**, 754 (1995).
[21]M. T. Rodgers, B. Walker, and P. B. Armentrout, Int. J. Mass Spectrom. **182–183**, 99 (1999).
[22]Y.-M. Chen and P. B. Armentrout, J. Chem. Phys. **103**, 618 (1995).
[23]M. R. Sievers, Y.-M. Chen, and P. B. Armentrout, J. Chem. Phys. **105**, 6322 (1996).
[24]M. R. Sievers and P. B. Armentrout, Int. J. Mass Spectrom. **179–180**, 103 (1998).
[25]M. R. Sievers and P. B. Armentrout, J. Phys. Chem. A **102**, 10754 (1998).
[26]M. R. Sievers and P. B. Armentrout, Inorg. Chem. **38**, 397 (1999).
[27]M. R. Sievers and P. B. Armentrout, Int. J. Mass Spectrom. **185–187**, 117 (1999).
[28]X.-G. Zhang and P. B. Armentrout, J. Phys. Chem. A **107**, 8904 (2003).
[29]X.-G. Zhang and P. B. Armentrout, J. Phys. Chem. A **107**, 8915 (2003).
[30]C. S. Hinton, F.-X. Li, and P. B. Armentrout, Int. J. Mass Spectrom. **280**, 226 (2009).
[31]F.-X. Li, K. Gorham, and P. B. Armentrout, J. Phys. Chem. A **114**, 11043 (2010).
[32]C. S. Hinton, M. Citir, M. Manard, and P. B. Armentrout, Int. J. Mass Spectrom. **308**, 265 (2011).
[33]C. S. Hinton, M. Citir, and P. B. Armentrout, "Guided ion-beam and theoretical studies of the reaction of Os^+ (^6D) with O_2: Adiabatic and nonadiabatic behavior," Int. J. Mass Spectrom. (published online).
[34]M. E. Weber, J. L. Elkind, and P. B. Armentrout, J. Chem. Phys. **84**, 1521 (1986).
[35]D. E. Clemmer, M. E. Weber, and P. B. Armentrout, J. Phys. Chem. **96**, 10888 (1992).
[36]N. F. Dalleska and P. B. Armentrout, Int. J. Mass Spectrom. Ion Process. **134**, 203 (1994).
[37]S. K. Loh, D. A. Hales, L. Lian, and P. B. Armentrout, J. Chem. Phys. **90**, 5466 (1989).
[38]R. H. Schultz and P. B. Armentrout, Int. J. Mass Spectrom. Ion Process. **107**, 29 (1991).
[39]E. Teloy and D. Gerlich, Chem. Phys. **4**, 417 (1974).
[40]D. Gerlich, Adv. Chem. Phys. **82**, 1 (1992).
[41]N. R. Daly, Rev. Sci. Instrum. **31**, 264 (1960).
[42]K. M. Ervin and P. B. Armentrout, J. Chem. Phys. **83**, 166 (1985).
[43]P. J. Chantry, J. Chem. Phys. **55**, 2746 (1971).
[44]P. B. Armentrout and F.-X. Li, J. Chem. Phys. **121**, 248 (2004).
[45]M. M. Armentrout, F.-X. Li, and P. B. Armentrout, J. Phys. Chem. A **108**, 9660 (2004).
[46]B. L. Kickel and P. B. Armentrout, J. Am. Chem. Soc. **117**, 4057 (1995).
[47]D. E. Clemmer, Y.-M. Chen, F. A. Khan, and P. B. Armentrout, J. Phys. Chem. **98**, 6522 (1994).
[48]C. L. Haynes and P. B. Armentrout, Organometallics **13**, 3480 (1994).
[49]B. L. Kickel and P. B. Armentrout, J. Am. Chem. Soc. **117**, 764 (1995).
[50]Y.-M. Chen, J. L. Elkind, and P. B. Armentrout, J. Phys. Chem. **99**, 10438 (1995).
[51]M. R. Sievers, Y.-M. Chen, J. L. Elkind, and P. B. Armentrout, J. Phys. Chem. **100**, 54 (1996).
[52]C. E. Moore, *Atomic Energy Levels*, NSRDS-NBS 35 (U.S. GPO, Washington, D.C., 1971).
[53]P. B. Armentrout, Int. J. Mass Spectrom. Ion Process. **200**, 219 (2000).
[54]W. J. Chesnavich and M. T. Bowers, J. Phys. Chem. **83**, 900 (1979).
[55]P. B. Armentrout, in *Advances in Gas Phase Ion Chemistry*, edited by N. Adams and L. M. Babcock (JAI Press, Greenwich, CT, 1992), Vol. 1, p. 83.
[56]F. Muntean and P. B. Armentrout, J. Chem. Phys. **115**, 1213 (2001).
[57]G. Herzberg, *Molecular Spectra and Molecular Structure* (Van Nostrand, New York, 1950).
[58]M. J. Frisch, G. W. Trucks, H. B. Schlegel *et al.*, Gaussian 09, Revision A.02, Gaussian, Inc., Pittsburgh, PA, 2009.
[59]A. D. Becke, J. Chem. Phys. **98**, 5648 (1993).
[60]C. Lee, W. Yang, and R. G. Parr, Phys. Rev. B **37**, 785 (1988).
[61]J. P. Perdew, Phys. Rev. B **33**, 8822 (1986).
[62]K. Raghavachari, G. W. Trucks, J. A. Pople, and M. Head-Gordon, Chem. Phys. Lett. **157**, 479 (1989).
[63]R. J. Bartlett, J. D. Watts, S. A. Kucharski, and J. Noga, Chem. Phys. Lett. **165**, 513 (1990).
[64]G. E. Scuseria and T. J. Lee, J. Chem. Phys. **93**, 5851 (1990).
[65]T. D. Crawford and J. F. Stanton, Int. J. Quantum Chem. **70**, 601 (1998).
[66]F. Furche and J. P. Perdew, J. Chem. Phys. **124**, 044103 (2006).
[67]T. G. Rowland, B. Sztáray, and P. B. Armentrout, J. Phys. Chem. A **117**, 1299–1309 (2013).
[68]M. W. Chase Jr., C. A. Davies, J. R. Downey Jr., D. J. Frurip, R. A. McDonald, and A. N. Syverud, J. Phys. Chem. Ref. Data **14**(Suppl. 1), 1 (1985).
[69]F. Weigend and R. Ahlrichs, Phys. Chem. Chem. Phys. **7**, 3297 (2005).
[70]D. Andrae, U. Haeussermann, M. Dolg, H. Stoll, and H. Preuss, Theor. Chim. Acta **77**, 123 (1990).
[71]D. Figgen, K. A. Peterson, M. Dolg, and H. Stoll, J. Chem. Phys. **130**, 164108 (2009).
[72]D. Feller, J. Comput. Chem. **17**, 1571 (1996).

[73]K. L. Schuchardt, B. T. Didier, T. Elsethagen, L. Sun, V. Gurumoorthi, J. Chase, J. Li, and T. L. Windus, J. Chem. Inf. Model. **47**, 1045 (2007).
[74]J. B. Foresman and A. E. Frisch, *Exploring Chemistry with Electronic Structure Methods*, 2nd ed. (Gaussian, Inc., Pittsburgh, PA, 1996).
[75]A. Halkier, T. Helgaker, P. Jørgensen, W. Klopper, and J. Olsen, Chem. Phys. Lett. **302**, 437 (1999).
[76]A. Halkier, T. Helgaker, P. Jørgensen, W. Klopper, H. Koch, J. Olsen, and A. K. Wilson, Chem. Phys. Lett. **286**, 243 (1998).
[77]A. Kramida, Yu. Ralchenko, J. Reader, NIST ASD Team, NIST Atomic Spectra Database (version 5.0) (National Institute of Standards and Technology, Gaithersburg, MD, 2012), see http://physics.nist.gov/asd, accessed 27 July 2013.
[78]G. Ohanessian, M. J. Brusich, and W. A. Goddard III, J. Am. Chem. Soc. **112**, 7179 (1990).
[79]D. Dai and K. Balasubramanian, J. Chem. Phys. **95**, 4284 (1991).
[80]M. C. Holthausen, C. Heinemann, H. H. Cornehl, W. Koch, and H. Schwartz, J. Chem. Phys. **102**, 4931 (1995).
[81]G. Gioumousis and D. P. Stevenson, J. Chem. Phys. **29**, 294 (1958).
[82]E. W. Rothe and R. B. Bernstein, J. Chem. Phys. **31**, 1619 (1959).
[83]M. D. Campbell-Miller and B. Simard, J. Opt. Soc. Am. B **13**, 2115 (1996).
[84]C. Yao, W. Guan, P. Song, Z. M. Su, J. D. Feng, L. K. Yan, and Z. J. Wu, Theor. Chem. Acc. **117**, 115 (2007).
[85]V. Brites, K. Franzreb, J. N. Harvey, S. G. Sayres, M. W. Ross, D. E. Blumling, A. W. Castleman, and M. Hochlaf, Phys. Chem. Chem. Phys. **13**, 15233 (2011).
[86]H. Lefebvre-Brion and R. W. Field, *The Spectra and Dynamics of Diatomic Molecules* (Elsevier, Amsterdam, 2004).
[87]J. Cao, W. J. Balfour, and C. X. W. Qian, J. Phys. Chem. A **101**, 6741 (1997).
[88]I. Kretzschmar, A. Fiedler, J. N. Harvey, D. Schröder, and H. Schwarz, J. Phys. Chem. A **101**, 6252 (1997).
[89]"Report on notation for the spectra of polyatomic molecules," J. Chem. Phys. **23**, 1997 (1955).
[90]C. Rue, P. B. Armentrout, I. Kretzschmar, D. Schroder, J. N. Harvey, and H. Schwarz, J. Chem. Phys. **110**, 7858 (1999).
[91]G. F. Stowe, R. H. Schultz, C. A. Wight, and P. B. Armentrout, Int. J. Mass Spectrom. Ion Process. **100**, 177 (1990).
[92]K. M. Ervin and P. B. Armentrout, J. Chem. Phys. **85**, 6380 (1986).
[93]K. M. Ervin and P. B. Armentrout, J. Chem. Phys. **90**, 118 (1989).
[94]P. B. Armentrout and F.-X. Li, "The bond energy of IrO^+: Guided ion-beam and theoretical studies of the reaction of Ir^+ (^5F) with O_2," J. Phys. Chem. A (published online).
[95]P. B. Armentrout, L. F. Halle, and J. L. Beauchamp, J. Chem. Phys. **76**, 2449 (1982).